2614 *Chem. Mater.* **2009,** *21,* 2614–2623
DOI:10.1021/cm900643e

CHEMISTRY OF MATERIALS
Article

Study of the Crystal Chemistry of the $n = 2$ Ruddlesden−Popper Phases $Sr_3FeMO_{6+\delta}$ (M = Fe, Co, and Ni) Using in Situ High Temperature Neutron Powder Diffraction

Liliana V. Mogni,[†] Fernando D. Prado,*[,†,§] Gabriel J. Cuello,[‡] and Alberto Caneiro[†]

[†]*Centro Atómico Bariloche, CNEA, S. C de Bariloche, 8400, Argentina, and* [‡]*Institut Laue-Langevin, BP 156, F-38042 Grenoble Cedex 9, France.* [§] *Actual address: Departamento de Física, Universidad Nacional del Sur, 8000 Bahía Blanca, Argentina*

Received September 7, 2008. Revised Manuscript Received April 18, 2009

Effects of the substitution of Fe by Co or Ni on the crystal structure of the $n = 2$ Ruddlesden−Popper phase $Sr_3Fe_2O_{6+\delta}$ have been studied by in situ high temperature neutron powder diffraction (NPD) in the temperature range 20 °C ≤ T ≤ 900 °C. The analysis of neutron diffraction data confirmed that for a given temperature the oxygen non-stoichiometry increases when Fe is replaced by Co or Ni. Oxygen vacancies were detected at the crystal sites O(1), connecting the octahedra along the *c*-axis, and O(3) in the FeO_2 planes of the perovskite layers. The substitution of Fe by Co or Ni increases the oxygen vacancy concentration at the O(3) crystal site, which were detected even when the total oxygen content was higher than 6.00. This result supports a diffusion mechanism involving the migration of oxide ions from the O(3) site to its adjacent empty O(1) sites and vice versa. The average linear expansion $\alpha_{ave} \approx {}^1/_3\,\alpha_{Vol}$ calculated from NPD data increases with the substitution of Fe by Co or Ni (19.9, 25.1, and 22.7 × 10^{-6} K^{-1} for M = Fe, Co and Ni, respectively). The expansion along the *c*-axis (α_c) affects mainly the perovskite block while the width of the rock-salt block remains constant. The crystal structure expansion is discussed considering the thermal and chemical contributions, along with the effect of the increasing delocalization of charge carriers when Fe is replaced with Co or Ni.

Introduction

The 3d transition metal oxides with perovskite-related intergrowth crystal structure include different systems with remarkable electrical and magnetic properties. For example, high-*Tc* superconductivity has been reported in the layered compound $La_{2-x}Ba_xCuO_4$,[1] while large negative magnetoresistance in $(La,Sr)_3Mn_2O_7$ [2] and other layered compounds[3,4] has been observed. Recently, the mixed conductor properties of the Ruddlesden−Popper (R-P) series of phases $(La,Sr)_{n+1}(Fe,B)_nO_{3n+1}$ with B = Fe, Co, Ni, Ti, Sc and $n = 2$ and 3 [5−11] have been explored to utilize these materials in electrochemical applications at high temperatures, such as solid oxide fuel cells and oxygen permeation membranes.[12] The crystal structure of the R-P phases consists of n perovskite layers $SrFeO_3$ alternating with SrO rock-salt layers (see Figure 1).[13,14] The crystal chemistry and defect structure at high temperatures of the parent compound $Sr_3Fe_2O_{6+\delta}$ have been already reported.[15,16] The crystal structure remains stable with tetragonal symmetry (S. G. *I*4/*mmm*) and tolerates a large oxygen non-stoichiometry without any structural transformation. The oxygen non-stoichiometry varies from $6+\delta = 6.00$ at $T = 1000$ °C and $pO_2 = 10^{-5}$ atm [14−16] to $6+\delta = 7.00$ when the sample is heat treated at $T = 500$ °C under an oxygen pressure of $P = 500$ atm.[14]

Aiming to increase the oxygen non-stoichiometry and thereby the oxide ion conductivity of the parent compound $Sr_3Fe_2O_{6+\delta}$, Fe has been replaced by Co or Ni.[5,7] Previous studies have shown that the solubility range of Co in the tetragonal crystal structure of the system

*To whom correspondence should be addressed. E-mail: fernando.prado@uns.edu.ar.

(1) Bednorz, J. C.; Muller, K. *Z. Phys. B* **1986**, *64*, 189.
(2) Moritomo, Y.; Asamitsu, A.; Kuwahara, H.; Tokura, Y. *Nature* **1996**, *380*, 141.
(3) Ghosh, S.; Adler, P. *Solid State Commun.* **2000**, *116*, 585.
(4) Motohashi, T.; Raveau, B.; Hervieu, M.; Maignan, A.; Pralong, V.; Nguyen, N.; Caignert, V. *J. Phys.: Condens. Matter* **2006**, *18*, 2157.
(5) Prado, F.; Armstrong, T.; Caneiro, A.; Manthiram, A. *J. Electrochem. Soc.* **2001**, *148*, J7.
(6) Manthiram, A.; Prado, F.; Armstrong, T. *Solid State Ionics* **2002**, *152−153*, 647.
(7) Mogni, L.; Prado, F.; Caneiro, A.; Manthiram, A. *Solid State Ionics* **2006**, *177*, 1807.
(8) Shilova, Y. A.; Patrakeev, M. V.; Mitberg, E. B.; Leonidov, I. A.; Kozhevnikov, V. L.; Poeppelmeier, K. R. *J. Solid State Chem.* **2002**, *168*, 275.
(9) Markov, A. A.; Patrakeev, M. V.; Kharton, V. V.; Pivak, Y. V.; Leonidov, I. A.; Kozhevnikov, V. L. *Chem. Mater.* **2007**, *19*, 3980.
(10) Lee, K. T.; Bierschenk, D. M.; Manthiram, A. *J. Electrochem. Soc.* **2006**, *153*, A1255.
(11) Lee, K. T.; Manthiram, A. *Chem. Mater.* **2006**, *18*, 1621.
(12) Bouwmeester, H. J. M.; Burggraaf, A. J. The CRC Handbook of Solid State Electrochemistry; Gellings, P. J, Bouwmeester, H. J. M., Eds.; CRC Press: Boca Raton, FL, 1997; Chapter 14.
(13) Ruddlesden, S. N.; Popper, P. *Acta Crystallogr.* **1958**, *11*, 54.
(14) Dann, S. E.; Weller, M. T.; Currie, D. B. *J. Solid State Chem.* **1992**, *97*, 179.
(15) Mogni, L.; Fouletier, J.; Prado, F.; Caneiro, A. *J. Solid State Chem.* **2005**, *178*, 2715.
(16) Prado, F.; Mogni, L.; Caneiro, A.; Cuello, G. *Solid State Ionics* **2007**, *178*, 77.

 Published on Web 05/21/2009

$Sr_3Fe_{2-x}Co_xO_{6+\delta}$ [17–20] is $0 \le x \le 1.75$. On the other hand, the substitution of Fe by Ni in the system $Sr_3Fe_{2-x}Ni_xO_{6+\delta}$ has been studied in the Ni content range $0 \le x \le 1$.[7,21,22] It was found that this cation substitution increases the electrical conductivity,[22] extends the range of oxygen non-stoichiometry ($5.5 \le 6+\delta \le 7$), [18,22] and improves the oxygen permeation flux across dense membranes,[7] which is related to oxide ion conductivity.[5] Similar effects were observed when Fe is partially replaced by the stable trivalent cation Sc.[9] On the contrary, the partial substitution of $Fe^{3+/4+}$ by Ti^{4+} decreases the oxygen non-stoichiometry range decreasing the oxide-ion conduction of the R-P phase.[8] The correlation observed between the oxygen vacancy concentration and the oxide-ion conduction in these R-P phases indicates that the oxide ion diffusion occurs via a vacancy mechanism.[23]

Neutron diffraction data of $Sr_3Fe_2O_{6+\delta}$ at high temperature have located the oxygen vacancies on the O(1) crystal sites connecting the octahedra along the *c*-axis and the O(3) crystal sites in the FeO_2 planes of the perovskite layers [14,16] (see Figure 1). This result agrees with a defect model proposed for $Sr_3Fe_2O_{6+\delta}$ to reproduce thermodynamic data.[15] Also, with the oxide ion diffusion mechanism proposed for $Sr_3Fe_{2-x}Ti_xO_{6+\delta}$ ($0 \le x \le 2$) [8] and $Sr_3Fe_{2-x}Sc_xO_{6+\delta}$ ($x = 0.2$ and 0.3) [9] involving oxygen jumps from the filled O(3) crystal site to an empty O(1) position.

In this paper we have studied the effects of the substitution of one molar of Fe by Co or Ni on the crystal structure and the oxygen vacancy concentration at crystal sites O(1), O(2), and O(3) of the $n = 2$ R-P phase $Sr_3Fe_2O_{6+\delta}$ using in situ NPD measurements in the temperature range 20 °C $\le T \le$ 900 °C, in air. In addition, the crystal structure expansion is analyzed considering the contribution of the thermal and chemical expansions along with the effect of the increasing delocalization of the charge carriers when Fe is replaced by Co or Ni.

Experimental Section

$Sr_3FeMO_{6+\delta}$ (M = Fe, Co, Ni) samples were prepared by an acetic acid based gel route using $SrCO_3$ (99.99%) and $M(CH_3COO)_2 \cdot xH_2O$ (99.9%) (M = Fe, Co, and Ni) as raw materials.[24] The water content of the acetates was determined by TGA prior to the synthesis. Stoichiometric amounts of the raw materials were dissolved in acetic acid and refluxed at $T = 80$ °C for approximately 2 h until a clear solution was obtained. The solutions were then heated in a hot plate to obtain a reddish transparent gel, which in turn was dried, decomposed at $T = 400$ °C during 30 min and heat treated at 900 °C in air for 24 h. Afterward, the powders were pressed and heat treated at $T = 1300$ °C for 24 h under flowing oxygen, then cooled down to room temperature at a rate of 1 °C/min with an intermediate heat treatment at $T = 400$ °C for 12 h to maximize the oxygen content.

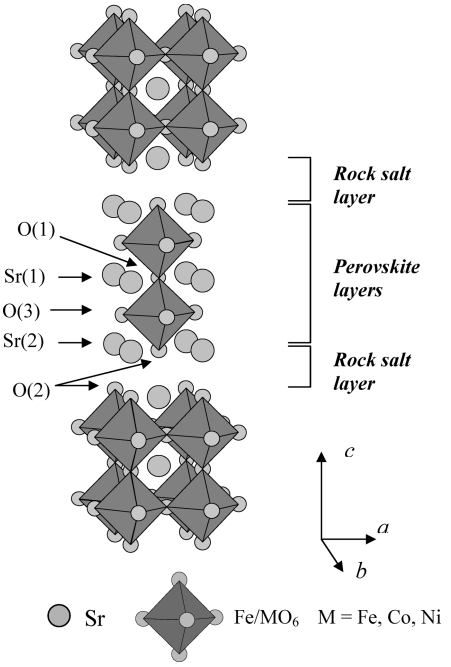

Figure 1. Crystal structure (S.G. *I*4/*mmm*) of Sr_3FeMO_7 (M = Fe, Co, Ni).

The final products were stored in a dessicator or in sealed glass tubes under vacuum at room temperature to prevent degradation with atmospheric water.[5,25] The samples were characterized by X-ray diffraction with a Philips PW 1700 diffractometer using Cu Kα radiation and a graphite monochromator. Data were collected over a range of $10° \le 2\theta \le 90°$ with a counting time of 2 s per step of 0.02°. X-ray powder diffraction patterns at room temperature indicated the $Sr_3FeMO_{6+\delta}$ (M = Fe, Co, Ni) samples were single phase. All the reflection peaks were indexed according to the tetragonal unit cell (S.G. *I*4/*mmm*) reported for this compound.[14] The homogeneity of the samples was confirmed by SEM observations and EDS analysis.

The neutron diffraction experiments were carried out at the Institute Lau-Langevin, Grenoble-France, on the D2B powder diffractometer at $T = 20$, 300, 500, 700, and 900 °C. Data were collected using the wavelength $\lambda = 1.594$ Å, in the angular range $10° \le 2\theta \le 140°$ with steps of 0.05°. The counting time was 4 h for all the patterns obtained at room temperature and at $T \ge 300$ °C for $Sr_3Fe_2O_{6+\delta}$ and $Sr_3FeNiO_{6+\delta}$, while it was 2 h for the patterns of $Sr_3FeCoO_{6+\delta}$ obtained at $T \ge 300$ °C. The high-resolution of this two-axis diffractometer allows a precise determination of the positions and occupation numbers of oxygen atoms. At room temperature, the samples were handled under flowing He and placed in a vanadium can. For NPD measurements at $T \ge 300$ °C, the samples were placed in a quartz tube open at the top in contact with air.

The NPD data were analyzed by the Rietveld method using the FullProf Program.[26] The profile of the diffraction peaks

(17) Prado, F.; Manthiram, A. *J. Solid State Chem.* **2001**, *158*, 307.
(18) Bréard, Y.; Michel, C.; Hervieu, M.; Studer, F.; Maignan, A.; Raveau, B. *Chem. Mater.* **2002**, *14*, 3128.
(19) Ghosh, S.; Adler, P. *J. Mater. Chem.* **2002**, *12*, 511.
(20) Veith, G. M.; Chen, R.; Popov, G.; Croft, M.; Shokh, Y.; Nowik, I.; Greenblatt, M. *J. Solid State Chem.* **2002**, *166*, 292.
(21) Mogni, L.; Prado, F.; Ascolani, H.; Abbate, M.; Moreno, M. S.; Manthiram, A.; Caneiro, A. *J. Solid State Chem.* **2005**, *178*, 1559.
(22) Mogni, L.; Prado, F.; Caneiro, A. *Chem. Mater.* **2006**, *18*, 4163.
(23) Islam, M. S. *J. Mater. Chem.* **2000**, *10*, 1027.
(24) Armstrong, T.; Prado, F.; Manthiram, A. *Solid State Ionics* **2001**, *140*, 89.
(25) Matvejeff, M.; Lehtimäki, M.; Hirasa, A.; Huang, Y.-H.; Yamauchi, H.; Karppinen, M. *Chem. Mater.* **2005**, *17*, 2775.
(26) Rodríguez-Carvajal, J. Fullprof 2000: A program for Rietveld Refinement and Profile Matching Analysis of Complex Powder Diffraction Patterns; Laboratoire Léon Brillouin (CEA-CNRS): Cedex, France, 2000.

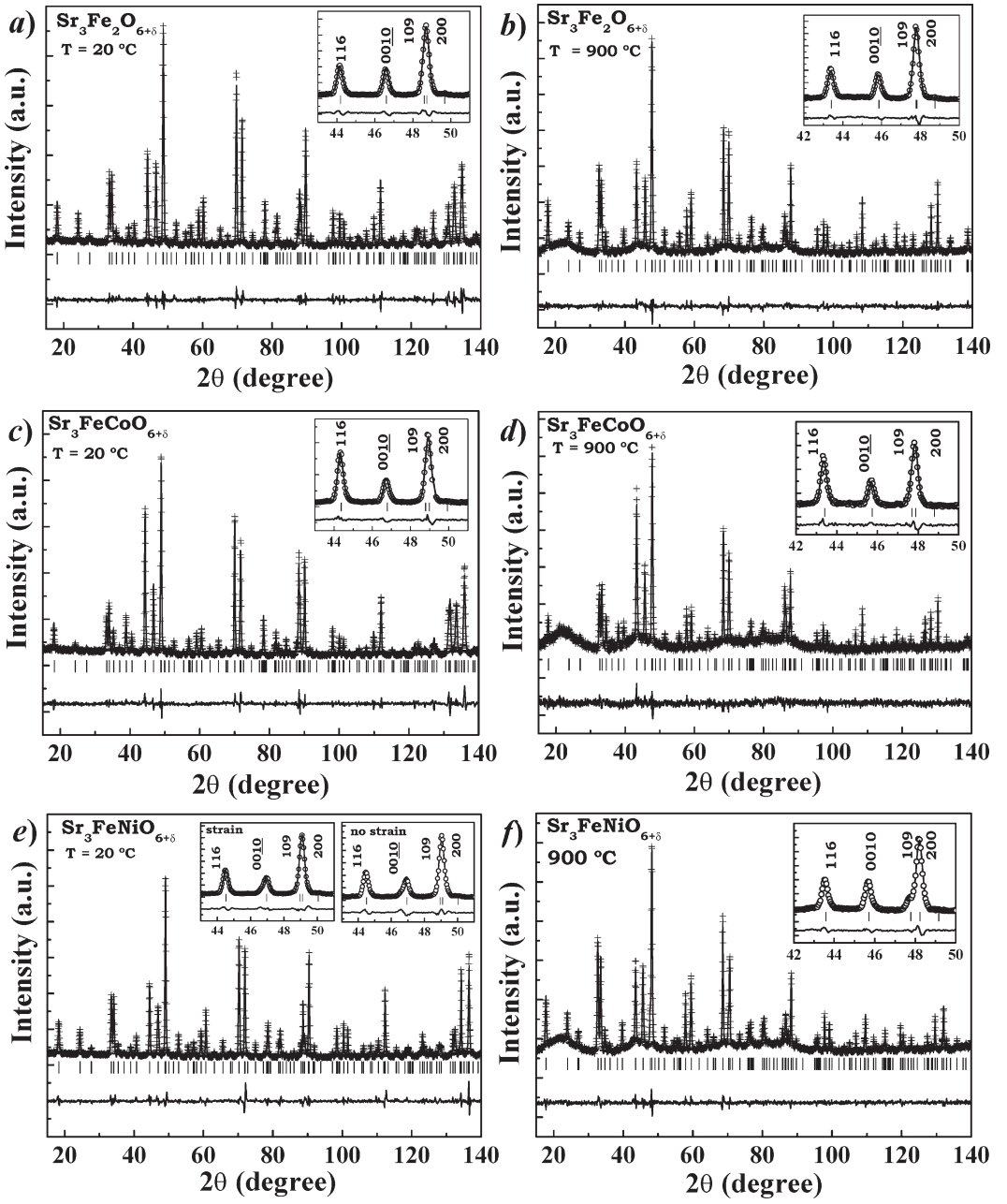

Figure 2. Powder neutron diffraction patterns of $Sr_3FeMO_{6+\delta}$ (M = Fe, Co, Ni) at room temperature (a, c, and e) and at T = 900 °C (b, d, and f) in air. Every figure includes the observed data (+), the calculated data (solid line), the difference plot (bottom), and the allowed reflections (marks) for the *I*4/*mmm* space group. The insets expand the 2θ range $42° \leq 2\theta \leq 50°$ to appreciate in more detail the quality of the refinements. The inset in panel "e" shows the refinements when the strain model for $Sr_3FeNiO_{6+\delta}$ at room temperature is considered and when it is neglected. The quality of the refinement improves when the strain model is included (see text).

was fitted using a Thompson−Cox−Hastings Pseudo-Voigt function.[26,27] The number of refined parameters varied between 21 and 27, while the number of reflections used during the refinements was around 110. The large concentration of oxygen vacancies observed in the $Sr_3FeMO_{6+\delta}$ (M = Fe, Co, Ni) system along with the presence of two different cations in the B site have led us to use the model of Stephens[24] for anisotropic peak broadening because of strain in the tetragonal cell.[26,28] The background of the NPD data obtained at 20 °C was adjusted by a fifth degree polynomial function, while linear interpolations of N selected points ($40 \leq N \leq 50$) were used for the patterns recorded at $T \geq 300$ °C, as a consequence of the quartz sample holder contribution to the baseline. The cell parameters, atomic positions, oxygen sites occupancies, and isotropic thermal parameters were modified during the refinement of the crystal structure. No correlation effects were found during the refinements between thermal parameters and oxygen occupancy. This fact was tested using different combinations of initial values for these parameters.

Results and Discussion

Crystal Structure. The crystal structures of the $Sr_3FeMO_{6+\delta}$ (M = Fe, Co, Ni) compounds were refined using the tetragonal space group *I*4/*mmm*.[14] Panels a, c, and e of Figure 2 display the NPD data, calculated profile, and the

(27) Thompson, P.; Cox, D. E.; Hastings, J. B. *J. Appl. Crystallogr.* **1987**, *20*, 79.
(28) Stephens, P. W. *J. Appl. Crystallogr.* **1999**, *32*, 281.

difference between them at $T = 20$ °C for $Sr_3Fe_2O_{6+\delta}$, $Sr_3FeCoO_{6+\delta}$, and $Sr_3FeNiO_{6+\delta}$, respectively. Panels b, d, and f of Figure 2 show the NPD data and the refined profile at $T = 900$ °C. The position of the allowed reflections of the tetragonal phase (S.G. *I*4/*mmm*) are also indicated in these figures.

No improvement was observed in the quality of the refinement for $Sr_3Fe_2O_{6+\delta}$ and $Sr_3FeCoO_{6+\delta}$ when the model for anisotropic strain was considered. On the contrary, R_{wp} and χ^2 clearly decrease when the anisotropic strain is included in the refinement of the crystal structure of the $Sr_3FeNiO_{6+\delta}$ sample at $T = 20$ and 300 °C. For instance, at $T = 20$ °C, R_{wp} and χ^2 decrease from 19.9 and 6.77 to 16.6 and 5.04, respectively. This result may be related to the larger number of oxygen vacancies that the crystal structure must incorporate at low temperature in $Sr_3FeNiO_{6+\delta}$ compared to the case of $Sr_3Fe_2O_{6+\delta}$ and $Sr_3FeCoO_{6+\delta}$ (see next section) because of the stabilization of Ni^{3+} rather than Ni^{4+} ions.[29] With increasing temperature ($T \geq 500$ °C) the anisotropic strain in $Sr_3FeNiO_{6+\delta}$ vanishes, likely because of the combination of thermal effects and the capacity to remove oxygen atoms from the crystal structure.

The structural parameters obtained for the $Sr_3FeMO_{6+\delta}$ (M = Fe, Co, Ni) samples at 20 and 900 °C are listed in Table 1 and 2, respectively. The variations with temperature of the lattice parameters *a* and *c* and unit cell volume (*V*) of $Sr_3FeMO_{6+\delta}$ (M = Fe, Co, Ni) are shown in Figure 3. At room temperature, the lattice parameters *a* and *c* decrease with the substitution of $Fe^{3+/4+}$ in the high spin configuration by the smaller $Co^{3+/4+}$ or Ni^{3+} in the intermediate or low spin configuration.[17,21] The expansion of the lattice parameters and unit cell volume with increasing temperature is a combination of the thermal expansion itself and the chemical expansion associated to the removal of oxygen atoms from the crystal structure. The increasing oxygen non-stoichiometry is revealed by a slope change in the *a*, *c*, or *V* versus *T* curves at approximately $T = 300$ °C where these transition metal oxides begin to lose oxygen.[5,15,22] As the temperature increases, the lattice parameter *c* of the $Sr_3FeCoO_{6+\delta}$ and $Sr_3FeNiO_{6+\delta}$ samples becomes larger than that of $Sr_3Fe_2O_{6+\delta}$.

In the next two sections, the oxide-ion diffusion mechanism and the expansion of the crystal structure are discussed based on the defect structure and the thermal and chemical expansions, respectively.

Oxygen Content and Diffusion Path. The total oxygen contents of the $Sr_3FeMO_{6+\delta}$ (M = Fe, Co, Ni) samples were determined from NPD data recorded at $T = 20$, 300, 500, 700, and 900 °C. These measurements allowed us to determine the occupancy factor of the oxygen crystallographic sites O(1), O(2), and O(3) in the $n = 2$ R-P phase crystal structure. In agreement with previous data,[14,16] the analysis of the NPD patterns obtained at high temperatures clearly locates the major concentration of oxygen vacancies on the O(1) (2a, 0,0,0) site connecting the octahedra along the *c*-axis. For a given temperature the sample containing Ni exhibits the larger concentration of oxygen vacancies on the O(1) site in the whole temperature range. At $T = 900$ °C they represent 54.5, 47.5, and 57% of the total sites for $Sr_3Fe_2O_{6+\delta}$, $Sr_3FeCoO_{6+\delta}$, and $Sr_3FeNiO_{6+\delta}$, respectively. The O(2) site located in the rock salt layer was found to be always fully occupied (occupancy factor of 1.00 ± 0.01) indistinctly of the transition metal. Even more interesting, the refinements of the crystal structures indicate the presence of a non-negligible concentration of oxygen vacancies in the

Table 1. Structural Parameters of $Sr_3FeMO_{6+\delta}$ (M = Fe, Co, Ni) at 20 °C[a]

sample	atom	site	*x*	*y*	*z*	occ	B_{iso} (Å^2)
$Sr_3Fe_2O_{6+\delta}$	Sr (1)	2*b*	0	0	1/2	1	0.88 (6)
$a = b = 3.8643$ (1)	Sr (2)	4*e*	0	0	0.3175 (1)	1	0.84 (4)
$c = 20.1490$ (3)	Fe/M	4*e*	0	0	0.0986 (1)	1	0.63 (3)
$6+\delta = 6.75$ (1)	O (1)	2*a*	0	0	0	0.75 (1)	0.7 (1)
$R_{wp} = 15.0$	O (2)	4*e*	0	0	0.1938 (1)	1	1.06 (5)
$\chi^2 = 3.25$	O (3)	8*g*	0	1/2	0.0928 (1)	1	1.05 (3)
$R_{Bragg} = 3.72$							
$Sr_3FeCoO_{6+\delta}$	Sr (1)	2*b*	0	0	1/2	1	0.86 (5)
$a = b = 3.8461$ (1)	Sr (2)	4*e*	0	0	0.3182 (1)	1	0.71 (4)
$c = 20.0800$ (3)	Fe/M	4*e*	0	0	0.0984 (1)	1	0.75 (4)
$6+\delta = 6.72$ (2)	O (1)	2*a*	0	0	0	0.72 (1)	1.1 (1)
$R_{wp} = 14.9$	O (2)	4*e*	0	0	0.1940 (1)	1	1.00 (5)
$\chi^2 = 3.32$	O (3)	8*g*	0	1/2	0.0918 (1)	1	0.99 (3)
$R_{Bragg} = 5.22$							
$Sr_3FeNiO_{6+\delta}$	Sr (1)	2*b*	0	0	1/2	1	0.85 (5)
$a = b = 3.8377$ (1)	Sr (2)	4*e*	0	0	0.3180 (1)	1	0.80 (4)
$c = 20.0125$ (2)	Fe/M	4*e*	0	0	0.0988 (1)	1	0.71 (3)
$6+\delta = 6.55$ (3)	O (1)	2*a*	0	0	0	0.63 (1)	0.78 (2)
$R_{wp} = 16.6$	O (2)	4*e*	0	0	0.1935 (1)	1	0.92 (5)
$\chi^2 = 5.04$	O (3)	8*g*	0	1/2	0.0917 (1)	0.98 (1)	0.93 (5)
$R_{Bragg} = 5.55$							

[a] The space group is tetragonal *I*4/*mmm* (# 139).

Table 2. Structural Parameters of $Sr_3FeMO_{6+\delta}$ (M = Fe, Co, Ni) at 900 °C[a]

sample	atom	site	*x*	*y*	*z*	occ	B_{iso} (Å^2)
$Sr_3Fe_2O_{6+\delta}$	Sr (1)	2*b*	0	0	1/2	1	2.65 (7)
$a = b = 3.9343$ (1)	Sr (2)	4*e*	0	0	0.3172 (1)	1	2.47 (5)
$c = 20.4635$ (3)	Fe/M	4*e*	0	0	0.1011 (1)	1	1.92 (3)
$6+\delta = 6.21$ (1)	O (1)	2*a*	0	0	0	0.43 (1)	4.4 (4)
$R_{wp} = 14.0$	O (2)	4*e*	0	0	0.1952 (1)	1	2.99 (6)
$\chi^2 = 2.67$	O (3)	8*g*	0	1/2	0.0893 (1)	0.944 (6)	2.76 (5)
$R_{Bragg} = 5.8$							
$Sr_3FeCoO_{6+\delta}$	Sr (1)	2*b*	0	0	1/2	1	2.7 (1)
$a = b = 3.9290$ (1)	Sr (2)	4*e*	0	0	0.3165 (2)	1	2.8 (1)
$c = 20.5162$ (4)	Fe/M	4*e*	0	0	0.1019 (2)	1	2.36 (7)
$6+\delta = 6.08$ (2)	O (1)	2*a*	0	0	0	0.53 (2)	7.3 (8)
$R_{wp} = 22.9$	O (2)	4*e*	0	0	0.1954 (3)	1	3.3 (1)
$\chi^2 = 1.29$	O (3)	8*g*	0	1/2	0.0889 (1)	0.89 (1)	3.2 (1)
$R_{Bragg} = 8.50$							
$Sr_3FeNiO_{6+\delta}$	Sr (1)	2*b*	0	0	1/2	1	2.84 (6)
$a = b = 3.9018$ (1)	Sr (2)	4*e*	0	0	0.3166 (1)	1	2.69 (4)
$c = 20.5202$ (2)	Fe/M	4*e*	0	0	0.1008 (1)	1	2.24 (2)
$6+\delta = 5.89$ (2)	O (1)	2*a*	0	0	0	0.43 (1)	7.4 (5)
$R_{wp} = 11.9$	O (2)	4*e*	0	0	0.1952 (1)	1	3.26 (5)
$\chi^2 = 1.91$	O (3)	8*g*	0	1/2	0.0880 (1)	0.864 (5)	3.05 (5)
$R_{Bragg} = 3.76$							

[a] The space group is tetragonal *I*4/*mmm* (# 139).

(29) Abbate, M.; Ascolani, H.; Mogni, L.; Prado, F.; Caneiro, A. *Physica B* **2004**, *354*, 7.

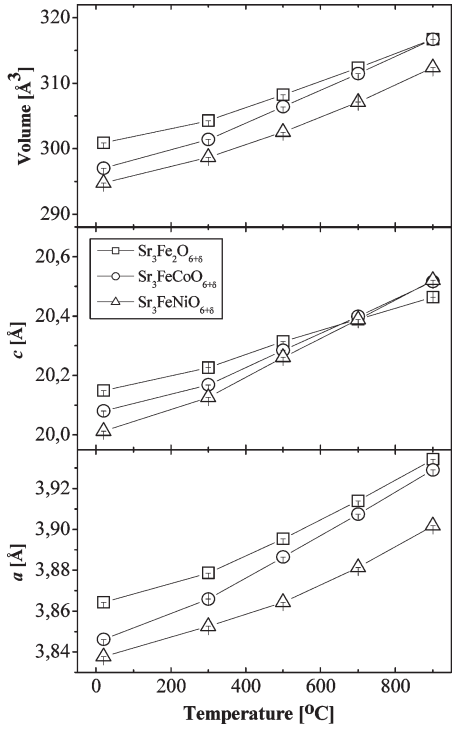

Figure 3. Lattice parameters and unit cell volume of $Sr_3FeMO_{6+\delta}$ (M = Fe, Co, Ni) as a function of temperature in air.

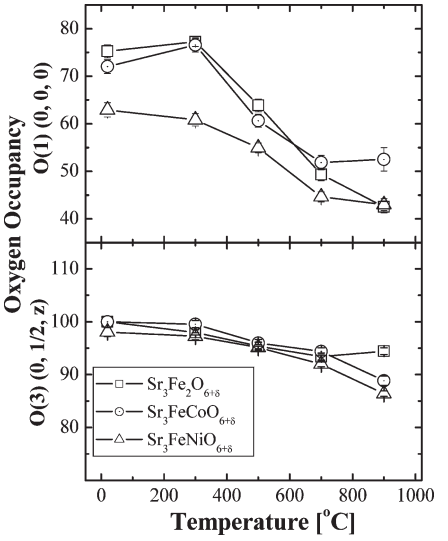

Figure 4. Variation of the occupancy factor of the O(1) (2a, 0,0,0) and O (3) (8g, 0, $^1/_2$, z) crystal sites with temperature in air.

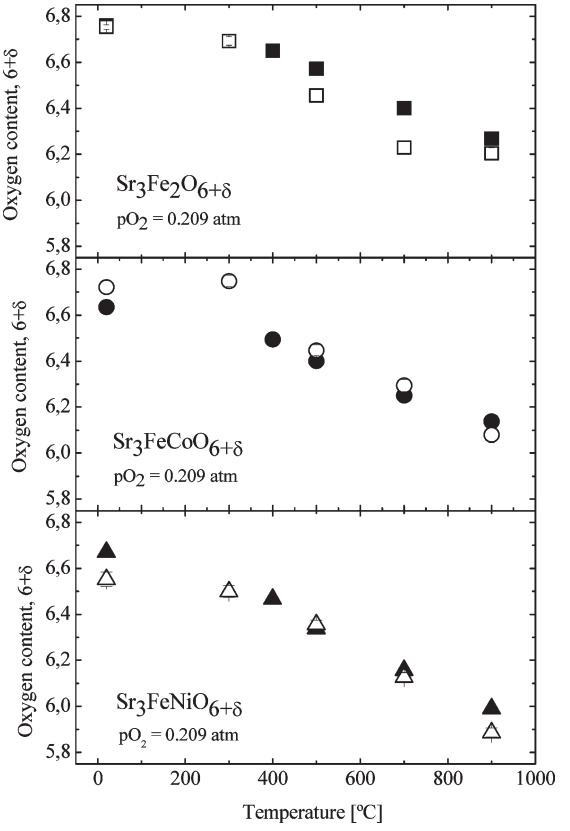

Figure 5. Variation of the total oxygen content of the $Sr_3FeMO_{6+\delta}$ (M = Fe, Co, Ni) samples with temperature obtaind from NPD data (open symbols). The solid symbols in the temperature range 400 °C ≤ T ≤ 900 °C correspond to the oxygen content values obtained from thermogravimetric measurements of the equilibrium pO_2 for pO_2 = 0.209 atm in a previous work.[22] The oxygen content values at T = 20 °C (solid symbols) were obtained by reducing the samples in dry H_2. Previous to the reduction process the samples were cooled in flowing O_2 with the same cooling rate used for the samples utilized during NPD measurements.

O(3) (8 g, 0, $^1/_2$, z) site in the $(Fe/M)O_2$ planes of the perovskite layers even when the total oxygen content is above 6.00. This result is analogous to that reported for $Sr_3Fe_2O_{6+\delta}$ [16] about the presence of oxygen vacancies on the O(3) crystal site. The oxygen vacancy concentration at this crystal site rises with increasing temperature reaching the values of 5.6, 11.2, and 13.6% at T = 900 °C for $Sr_3Fe_2O_{6+\delta}$, $Sr_3FeCoO_{6+\delta}$, and $Sr_3FeNiO_{6+\delta}$, respectively. Figure 4 shows the variations of the occupancy factor on the O(1) and O(3) crystal sites with temperature for the three compositions.

The quality of the refinement lessens when the model assumes that both the O(3) site is fully occupied and oxygen vacancies are located only on the O(1) site. For example, for $Sr_3FeNiO_{6+\delta}$ at 700 °C, the R_{wp} and χ^2 parameters increase their values from 11.9 and 2.35 to 12.4 and 2.56, respectively, if the O(3) site is considered fully occupied. Similar behavior was observed for the other compounds apart from $Sr_3Fe_2O_{6+\delta}$ at 20 °C and $Sr_3FeCoO_{6+\delta}$ at 20 and 300 °C. For these particular cases in the low temperature range, the quality of the refinements slightly improves if the O(3) site is assumed fully occupied.

Figure 5 shows the variation of the total oxygen content ($6+\delta$) with temperature for the $Sr_3FeMO_{6+\delta}$ (M = Fe, Co, Ni) samples obtained from NPD data. These data are compared to oxygen content values obtained from thermogravimetric measurements of the equilibrium oxygen partial pressure (pO_2) at identical conditions of T and pO_2.[22] Both sets of data show quite a good agreement for $Sr_3FeCoO_{6+\delta}$ and $Sr_3FeNiO_{6+\delta}$, while some differences are observed at 500 and 700 °C for $Sr_3Fe_2O_{6+\delta}$. The total oxygen content decreases when the temperature rises and also with the substitution of Fe by Co or Ni according to the series Ni < Co ≈ Fe.

The isotropic thermal factors for the O(1) oxygen atom of $Sr_3FeCoO_{6+\delta}$ and $Sr_3FeNiO_{6+\delta}$ at T = 900 °C (B_{iso} = 7.3−7.4 Å^2) are larger than the ones obtained at room

Table 3. Transition Metal−oxygen Bond Distances and Their Statistical Errors Calculated from NPD Data

		20 °C	300 °C	500 °C	700 °C	900 °C
$Sr_3Fe_2O_{6+\delta}$	Fe−O(1)	1.986 (2)	1.995 (1)	2.025(2)	2.059 (2)	2.069 (2)
	Fe−O(2)	1.919 (3)	1.931 (2)	1.930(5)	1.923 (5)	1.926 (5)
	Fe−O(3)	1.936 (1)	1.943 (1)	1.955 (1)	1,970 (1)	1.982 (1)
$Sr_3FeCoO_{6+\delta}$	(Fe/Co)−O(1)	1.976 (2)	1.995 (2)	2.032 (2)	2.058 (4)	2.091 (4)
	(Fe/Co)−O(2)	1.920 (3)	1.924 (3)	1.919 (5)	1.928 (6)	1.918 (7)
	(Fe/Co)−O(3)	1.928 (1)	1.939 (1)	1.953 (1)	1.968 (1)	1.983 (1)
$Sr_3FeNiO_{6+\delta}$	(Fe/Ni)−O(1)	1.977 (2)	1.999 (2)	2.019 (1)	2.042 (1)	2.069 (2)
	(Fe/Ni)−O(2)	1.895 (4)	1.904 (5)	1.924 (2)	1.925(2)	1.936 (3)
	(Fe/Ni)−O(3)	1.924 (1)	1.933 (1)	1.942 (1)	1.955 (1)	1.969 (1)

temperature and than those obtained for the O(1) oxygen atom in $Sr_3Fe_2O_{6+\delta}$ at 900 °C (see Tables 1 and 2). Large thermal factors are found in ionic conductors where the localization of the conducting ions may be difficult. For example, Goutenoire et al. [30] have reported isotropic thermal factors for the oxygen atoms of the compound β-$La_2Mo_2O_9$ at T = 617 °C ranging between 5.2 and 13 Å^2. Hence, the B_{iso} parameter for the O(1) oxygen atoms observed for $Sr_3FeCoO_{6+\delta}$ and $Sr_3FeNiO_{6+\delta}$ are likely related to the increasing oxygen ion mobility in these compounds compared to that in $Sr_3Fe_2O_{6+\delta}$.

In Table 3 the (Fe/M)−O bond distances obtained from NPD data at various temperatures are listed. It can be observed that the apical (Fe/M)−O(2) bond is shorter than both the (Fe/M−O(1)) and the in-plane (Fe/M−O(3)) bonds at all the temperatures for the three compounds. The rise of temperature causes the expansion of all the M−O bonds, although the relative expansion is lesser for the M−O(2) bond. This behavior suggests that the M−O(2) bond is stronger than the others in agreement with the formation of oxygen vacancies only on the O(1) and O(3) crystal sites.

Recently, Markov et al.[9] have discussed the formation of oxygen vacancies in the crystal structure of the n = 2 R-P phases $Sr_3Fe_{2-x}Sc_xO_{7-\delta}$ ($0 \le x \le 0.3$). They have found from static-lattice simulation studies that the oxygen vacancy formation is more favorable on the O(1) crystal site, while the energy required for creating oxygen vacancies on the O(3) sites is slightly larger than that obtained for the O(1) site. However, the energy formation values in both cases are close enough to allow the presence of oxygen vacancies on both crystal sites, particularly at high temperatures. In contrast, the energy needed to create an oxygen vacancy on the O(2) crystal site is high enough to justify its full occupancy.[9]

Oxygen vacancies on the O(3) crystal site have also been reported for Sr_3FeCoO_{7-y} with y = 1.55 and 1.1 [18] and $Sr_3Co_2O_{5+z}$ with z = 0.91, 0.64, and 0.38.[31,32] These results were obtained from NPD data carried out at room temperature on samples with controlled oxygen content below 6.00.[18,31,32] Instead, our results indicate that the crystal structure of the R-P phases $Sr_3FeMO_{6+\delta}$ (M = Fe, Co, Ni) contains oxygen vacancies on the O(3) sites also when the total oxygen content is higher than 6.00, which supports previous thermodynamic measurements,[22] and the oxide ion diffusion mechanism via oxygen vacancies.[8,9]

Table 4. Distances between Oxygen Atoms and Their Statistical Errors at Different Crystallographic Sites at T = 900 °C Obtained from NPD Data

	$d_{O(1)-O(1)'}$ (Å)	$d_{O(3)-O(3)'}$ (Å)	$d_{O(1)-O(3)}$ (Å)
$Sr_3Fe_2O_{6+\delta}$	3.9343(1)	2.7820(1)	2.685(1)
$Sr_3FeCoO_{6+\delta}$	3.9290(1)	2.7782(1)	2.681(1)
$Sr_3FeNiO_{6+\delta}$	3.9018(1)	2.7590(1)	2.6586(1)

Usually the oxide ion diffusion in perovskites or perovskite related intergrowth oxides with mixed valence transition metals occurs via an oxygen vacancy mechanism, since the formation and migration of interstitial oxide ions is unfavorable in these crystal structures.[23]

The large oxygen vacancy concentration ($0 \le 1+\delta \le 1.50$) induced with the substitution of Fe by Co or Ni and the decreasing ionic conductivity when Fe^{4+}/Fe^{3+} is partially replaced by Ti^{4+} in $Sr_3Fe_2O_{6+\delta}$[8] are strong evidence that the ionic conduction in the $Sr_3FeMO_{6+\delta}$ (M = Fe, Co, and Ni) phases takes place via an oxygen vacancy mechanism.

The existence of oxygen vacancies at the O(1) and O(3) crystal sites suggests that the mechanism for oxide ion diffusion may involve the pathways O(1)→O′(1), O(1)→O′(3), and O(3)→O′(3) jumps, where O′(1) and O′(3) indicate empty neighbor sites. In Table 4 the distances between oxygen atoms calculated from NPD data at T = 900 °C for $Sr_3FeMO_{6+\delta}$ (M = Fe, Co, Ni) are listed. The large distance of the O(1)→O′(1) jump (see Table 4) along with the limited room available for the oxygen atom to get through two adjacent Sr(1) atoms (~1 Å) permitted us to rule out this option.[8,9,16] On the other hand, the distance $d_{O(1)\rightarrow O(3)}$ is shorter than $d_{O(3)\rightarrow O(3')}$ by ~0.1 Å, and the diameter of the bottleneck defined by the atoms Sr(1)-(Fe/M)-Sr(1) and Sr(1)-(Fe/M)-Sr(2) is approximately ~2 Å. Although this result suggests that the O(1)→O(3) and O(3)→O(3′) jumps are maybe very similar, static-lattice simulations [9] have indicated a lower migration energy (1.2 eV) for the O(1)↔O(3) jumps than for the O(3)↔O′(3) jumps (1.8 eV) in $Sr_3Fe_{2-x}Sc_xO_{7-\delta}$. Therefore, the O(1)↔O(3) jumps may be the predominant mechanism for oxygen diffusion in the $Sr_3FeMO_{6+\delta}$ (M = Fe, Co, Ni) compounds.

(30) Goutenoire, F.; Isnard, O.; Retoux, R.; Lacorre, P. *Chem. Mater.* **2000**, *12*, 2575.
(31) Viciu, L.; Zandbergen, H.; Xu, Q.; Huang, Q.; Lee, M.; Cava, R. J. *J. Solid State Chem.* **2006**, *179*, 501.
(32) Hill, J. M.; Dabrowski, B.; Mitchell, J. F.; Jorgensen, J. D. *Phys Rev. B* **2006**, *74*, 174417.

Experimental data of the ionic conductivity of these mixed conductors were obtained through oxygen permeability measurements[5,7] on ceramic membranes. These data indicate that the oxygen flux across the membrane (jO_2) is bulk limited[5] for $La_{0.3}Sr_{2.7}FeCoO_{6+\delta}$ and that the ionic conductivity values, σ_i, vary between 0.01 and 0.05 S cm^{-1} at 900 °C. In spite of the 2D character of the oxide ion diffusion in the R-P phases, these values are similar to those obtained for some cubic perovskites like $La_{0.4}Sr_{0.6}Co_{0.8}Fe_{0.2}O_{3-\delta}$[5] but lower than those reported for $SrCo_{0.8}Fe_{0.2}O_{3-\delta}$[5] and $Sr_{0.5}Ba_{0.5}Co_{0.8}Fe_{0.2}O_{3-\delta}$.[33] Other very important factors that influence σ_i values are the oxygen vacancy concentration and the jump distance during the diffusion process.[34] Regarding the R-P phases, the substitution of Fe by Co or Ni has two clear effects; on one hand it reduces the atomic distances $d_{O(1)-O(3)}$ and $d_{O(3)-O(3)'}$ and on the other, the total oxygen vacancy concentration increases according to the series $Sr_3Fe_2O_{6+\delta} < Sr_3FeCoO_{6+\delta} < Sr_3FeNiO_{6+\delta}$. The combination of both effects is responsible for the increase in the oxide ion conductivity observed in a previous work in $La_{0.3}Sr_{2.7}Fe_2O_{6+\delta}$ when Fe is replaced by Co or Ni.[7]

Thermal and Chemical Expansion. The total expansion coefficients associated to the crystal structure were calculated using the general expression

$$\alpha_p = \left.\frac{p - p_0}{p_0 \Delta T}\right|_{pO_2 = cte} \quad (1)$$

in which p stands for the lattice parameters a and c or the unit cell volume V, p_0 corresponds to parameters values at a temperature of reference, and ΔT is the temperature range in which the expansion coefficient is evaluated. The reference values were chosen at 20 °C. In Table 5 are listed the total expansion coefficients for the lattice parameters a and c and the average linear expansion $\alpha_{ave} = {}^1/_3\, \alpha_{Vol}$ calculated from NPD data in the temperature range 20 °C $\leq T \leq$ 900 °C. These data show that while the total expansion coefficient for the c axis, α_c, increases with the series $\alpha_c^{Fe} < \alpha_c^{Co} < \alpha_c^{Ni}$, the expansion coefficients α_a and α_{ave} exhibit a maximum for the sample containing Co.

The total expansion coefficient in transition metal oxides incorporates both the effects of thermal and chemical expansion. This last expansion effect is related to the variation of the oxygen content with temperature and oxygen partial pressure.[35,36] The thermal expansion coefficient, α_p^T, is defined at constant pressure and oxygen content (x_v):

$$\alpha_p^T = \left(\frac{\partial \ln(p)}{\partial T}\right)_{x_V, P} \quad (2)$$

Table 5. Expansion Coefficients Evaluated from NPD Data Using the Lattice Parameters *a* and *c* at 20 and 900 °C

	α_a (10^{-6} K^{-1})	α_c (10^{-6} K^{-1})	$\alpha_{ave} = \alpha_{Vol}/3$ (10^{-6} K^{-1})
$Sr_3Fe_2O_{6+\delta}$	20.6(1)	17.7(1)	19.9 (1)
$Sr_3FeCoO_{6+\delta}$	24.5(1)	24.7(1)	25.1 (1)
$Sr_3FeNiO_{6+\delta}$	19.0(1)	28.8(1)	22.7 (1)

while the chemical expansion coefficient, $\alpha^{x_V}{}_p$, is defined at constant T and P as

$$\alpha_p^{x_V} = \left(\frac{\partial \ln(p)}{\partial x_V}\right)_{T, P} \quad (3)$$

The thermal expansion contribution defined by eq 2 is associated with nonsymmetrical properties of the interatomic potential.[37] A simple model based on the Morse potential has been used to describe the interatomic potential of ionic and covalent materials.[38] The evaluation of a set of materials with a bonding character varying widely from ionic to covalent has shown that the thermal expansion decreases with the increasing covalent character of the material.[38] In addition, the analysis of thermodynamic data for the $n = 2$ R-P phases $Sr_3FeMO_{6+\delta}$ (M = Fe, Co, Ni) have indicated an increasing charge carrier delocalization with the substitution of Fe by Co or Ni.[22] This behavior was associated to the increasing covalent character of the M−O bond. Therefore, the thermal expansion of the $n = 2$ R-P phases should decrease as the covalency of the M−O bond increases with the partial replacement of Fe by Co or Ni.

The chemical expansion defined by eq 3 takes into account the variation of interatomic distances at a constant temperature because of changes in the oxygen nonstoichiometry. This effect is related with the variation of the transition metal ionic radii and with the presence of local lattice distortions and/or preferred coordination.[36] It is possible to evaluate the chemical expansion of the $Sr_3Fe_2O_{6+\delta}$ phase using in situ XRD data reported in ref 5 at 900 °C in the oxygen partial pressure range 10^{-5} atm $\leq pO_2 \leq 1$ atm and also from NPD data at room temperature on samples with controlled oxygen content.[14] Both sets of data clearly show that the increase of the oxygen vacancy concentration causes a positive expansion of the lattice parameter a and a negative expansion of the lattice parameter c. The behavior of the lattice parameter a can be assigned to the higher ionic radii of Fe^{3+} ($r_{Fe}{}^{3+} = 0.645$ Å, high spin, coordination VI) compared to Fe^{4+} ionic radii ($r_{Fe}{}^{4+} = 0.585$ Å, high spin, coordination VI).[39] In the case of the c-axis, the removal of oxygen atoms from the O(1) crystal site leads to two opposite effects whose combination controls the chemical expansion of the c-axis for $Sr_3Fe_2O_{6+\delta}$ (see Figure 6). On one hand, a lower formal oxidation state of Fe increases its ionic radii expanding the c-axis. On the other hand the empty O(1) site behaves like a

(33) Shao, Z.; Yang, W.; Cong, Y.; Dong, H.; Tong, J.; Xiong, G. *J. Membr. Sci.* **2000**, *172*, 177.
(34) Kilner, J. A. *Solid State Ionics* **2000**, *129*, 13.
(35) McIntosh, S.; Vente, J. F.; Haije, W. G.; Blank, D. H. A.; Bouwmeester, H. J. *Solid State Ionics* **2006**, *177*, 833–842.
(36) Chen, X.; Yu, J.; Adler, S. B. *Chem. Mater.* **2005**, *17*, 4537.
(37) Kittel, C. Introduction to Solid State Physics, 7th ed.; John Wiley & Sons: New York, 1996.
(38) Ruffa, A. *J. Mater. Sci.* **1980**, *15*, 2258.
(39) Shannon, R. D. *Acta Crystallogr.* **1976**, *A32*, 751.

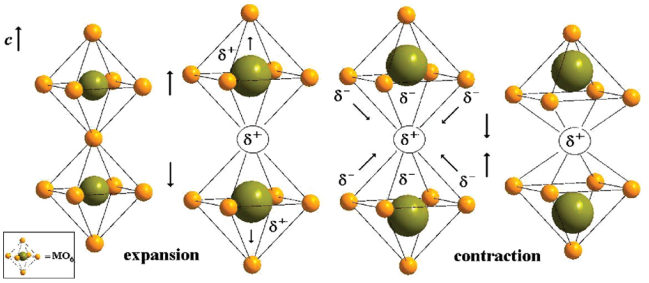

Figure 6. Schematic of the expansion−contraction of the perovskite layers in the $Sr_3FeMO_{6+\delta}$ compound when an oxygen vacancy is located at the O(1) site. The increase of the ionic radii of the transition metal causes the expansion of the *c*-axis. On the other hand, the oxygen atoms at the O(3) sites are attracted by the empty O(1) site, reducing the *c*-axis. The arrows indicate the atomic displacement.

positive charge causing the relaxation of the surrounding ions.[40] Thus, the O(3) oxygen ions are attracted by the empty O(1) site giving place to a contraction of the *c*-axis, while the Fe cations move outward on the *c*-axis remaining over the square base of the pyramidal coordination formed by O(3) oxygen atoms (see Figure 6). The negative expansion of the *c*-axis indicates that the atomic relaxation effect prevails over the expansion effect.

The total expansion behavior of $Sr_3FeCoO_{6+\delta}$ follows a similar scheme. The lattice parameters at room temperature obtained from NPD data on samples with $6+\delta = 5.90$ and $6+\delta = 6.90$ [18] are listed in Table 6 along with the calculated chemical expansion coefficients for both the *a* and *c* directions. For comparison we have included the lattice parameter values of $Sr_3Fe_2O_{6+\delta}$ obtained from NPD data.[14] In both cases the oxygen content variation is equivalent, which allows us to analyze the transition metal substitution effect on the chemical expansion. The substitution of Fe by Co reduces the lattice parameters *a* and *c* because of the smaller ionic radii of Co. For $Sr_3FeCoO_{6+\delta}$, the increase of the oxygen vacancy concentration changes the formal oxidation state of Fe and Co modifying their ionic radii. For example the ionic radii changes from 0.585 Å to 0.645 Å when the oxidation state of Fe changes from Fe^{4+} to Fe^{3+} in the high spin configuration. The ionic radii of Co cations varies from 0.53 Å to 0.61 Å when the oxidation state changes from Co^{4+} to Co^{3+} in the high spin configuration.[39] The variation of the Co ionic radii is larger than that expected for the Fe cation, in agreement with the larger chemical expansion in the *a* direction reported for $Sr_3FeCoO_{6+\delta}$ compared to that observed for $Sr_3Fe_2O_{6+\delta}$ (see Table 6). On the other hand, the chemical expansion of the lattice parameter *c* of $Sr_3FeCoO_{6+\delta}$ is positive. This behavior is opposite to the negative variation observed for $Sr_3Fe_2O_{6+\delta}$, which can be explained considering the higher delocalization of the charge carriers in $Sr_3FeCoO_{6+\delta}$ compared to $Sr_3Fe_2O_{6+\delta}$.[22] We believe that the charge carrier delocalization in $Sr_3FeCoO_{6+\delta}$ may help to reduce the local electrostatic interactions, caused by the oxygen vacancies, and therefore the lattice distortion associated to them

(40) Swalin, R. Thermodynamics of Solids; John Wiley & Sons: New York, 1962.

Table 6. Chemical Expansion Coefficients at $T = 20$ °C Obtained from Data Reported in the Literature for $Sr_3Fe_2O_{6+\delta}$ [22] and $Sr_3FeCoO_{6+\delta}$ [25] [a]

	$6+\delta$	*a* (Å)	*c* (Å)	$\alpha_a^{x_V}$	$\alpha_c^{x_V}$
$Sr_3Fe_2O_{6+\delta}$	6.00	3.8940	20.0396	**+0.075**	**-0.038**
	7.00	3.8526	20.1490		
$Sr_3FeCoO_{6+\delta}$	5.90	3.8786	20.1195	**+0.098**	**+0.033**
	6.90	3.8403	20.025		

[a] The values were obtained using eq 3.

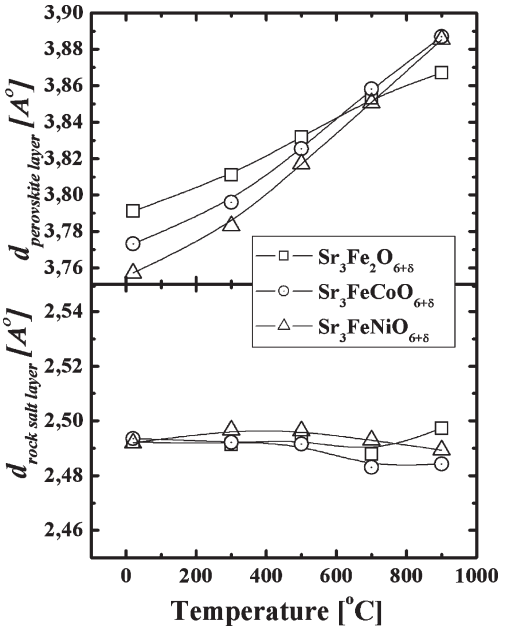

Figure 7. Expansion of the perovskite and rock salt layers with temperature (see details in the text).

(see Figure 6). For this reason the effect of the ionic radii change prevails on the lattice polarization effect giving place to a positive chemical expansion along the *c*-axis. No data of the crystal structure variation with the oxygen content at constant temperature are available for $Sr_3FeNiO_{6+\delta}$. However, thermodynamic data[22] suggest that the charge carriers are as delocalized as in $Sr_3FeCoO_{6+\delta}$ predicting a similar behavior for the chemical expansion.

The total expansion coefficients listed in Table 5 contain both thermal and chemical effects. The variation of the oxygen vacancies concentration on the O(1) sites in the evaluated temperature range is larger for $Sr_3Fe_2O_{6+\delta}$ (~30%) than those observed for $Sr_3FeCoO_{6+\delta}$ and $Sr_3FeNiO_{6+\delta}$ (~20%, see Figure 4). According to the analysis above we expect that the chemical expansion along the *c* direction would vary according to the series $\alpha^{x_V}{}_c(Fe) < \alpha^{x_V}{}_c(Co) < \alpha^{x_V}{}_c(Ni)$, while the thermal expansion would decrease according to the relation $\alpha_c^T(Fe) > \alpha_c^T(Co) > \alpha_c^T(Ni)$ because the covalent character of the M−O bond increases. The experimental values obtained for the total expansion along the *c*-axis ($\alpha_c(Fe) < \alpha_c(Co) < \alpha_c(Ni)$) indicate that the chemical expansion prevails over the thermal expansion. Extra information can be obtained by analyzing how the expansion along the *c*-axis of the crystal structure is absorbed by the perovskite and rock-salt layers. In Figure 7 the variations of the width of the perovskite layer (d_p)

and the rock-salt layer (d_{rs}) with temperature for $Sr_3FeMO_{6+\delta}$ (M = Fe, Co and Ni) are shown. Both distances d_p and d_{rs} were calculated using eqs 4 and 5, respectively:

$$d_p = \left[z_{Sr(1)} - \frac{z_{Sr(2)} + 1/2 - z_{O(2)}}{2} \right] \times c \quad (4)$$

$$d_{rs} = (z_{Sr(2)} - z_{O(2)}) \times c \quad (5)$$

Noteworthy, the width of the rock salt layer remains practically constant for the three compounds in the whole temperature range, while the width of the perovskite layer increases with rising temperature in agreement with the earlier discussion related with the expansion−contraction effects in the perovskite layer.

The total expansion coefficient along the *a* direction shows no correlations with the oxygen vacancies concentration on the O(3) site, which follows the series Fe < Co < Ni. The experimental data reveal a maximum expansion coefficient value for $Sr_3FeCoO_{6+\delta}$ (see Table 5). This seems to be caused by a combination of (a) increasing covalence of the M−O bond, which reduces the thermal expansion with the series α_a^T(Ni) < α_a^T(Co) < α_a^T(Fe), and (b) the larger ionic radii variation of the Co and Ni ions compared to Fe, when oxygen atoms are removed from the crystal structure, which leads to an increasing chemical expansion according to the relation $\alpha^{x_V}{}_a$(Fe) < $\alpha^{x_V}{}_a$(Co) < $\alpha^{x_V}{}_a$(Ni).

Recently, Lee et al. [11] have reported linear expansion data on the $n = 2$ R-P phases $Sr_{3-x}La_xFe_{2-y}Co_yO_{6+\delta}$ with $0 \le x \le 0.6$ and $0 \le y \le 0.6$ in the temperature range $0 \le T \le 800$ °C. The total expansion coefficient increases from 17.4 to 21.1 × 10^{-6} K^{-1} as the Co content increases. These values are slightly lower than those we have obtained for $Sr_3FeMO_{6+\delta}$ (M = Fe, Co, Ni) due likely to the incorporation of La in the crystal structure and differences in the temperature range.[11] The effect of the replacement of Fe by Co on the linear expansion ($\Delta L/L$) reported by Lee et al. [11] agrees with the trend we have obtained for α_{ave} (see Table 5). The authors have explained this behavior based on two effects: (a) the increase of the oxygen non-stoichiometry with increasing Co content and (b) the transition from low-spin (LS) to high-spin (HS) electronic configuration with increasing temperature.

The average linear expansion coefficient values $\alpha_{ave} \approx {}^1/_3\ \alpha_{Vol}$ obtained from NPD data for the R-P phases $Sr_3Fe_2O_{6+\delta}$, $Sr_3FeCoO_{6+\delta}$, and $Sr_3FeNiO_{6+\delta}$ were 19.9, 25.1, and 22.7 × 10^{-6} K^{-1}, respectively. These values are comparable with those obtained from dilatometry measurements for $La_{1-x}Sr_xCo_{1-y}Fe_yO_{3-\delta}$ samples with $x = 0.7$ and Fe content in the range $0 \le y \le 1$ and samples with a varying Sr content in the range $0 \le x \le 0.9$ with $y = 0$. Similar values were obtained for $Ba_xSr_{1-x}Co_{1-y}Fe_yO_{3-\delta}$ samples with $x = 0.5$ and $0.2 \le y \le 0.8$ or $y = 0.2$ and $0 \le x \le 0.8$ where the total linear expansion coefficient values vary from 18.5 to 27.1 × 10^{-6} K^{-1}.[41,42]

(41) Tietz, F.; Arul Raj, I.; Zahid, M.; Stöver, D. *Solid State Ionics* **2006**, *177*, 1753.
(42) Zhu, Q.; Jin, T.; Wang, Y. *Solid State Ionics* **2006**, *177*, 1199.

Conclusions

The oxygen defect structures of the $n = 2$ R-P phases $Sr_3FeMO_{6+\delta}$ (M = Fe, Co, Ni) have been determined through the analysis of in situ high temperature NPD in the temperature range 20 °C ≤ *T* ≤ 900 °C in air. The refinement of NPD data reveals the presence of a non-negligible concentration of oxygen vacancies on the O(3) sites in the FeO_2 planes of the perovskite layers, along with oxygen vacancies located on the O(1) sites linking the octahedra between perovskite layers. The finding of oxygen vacancies on the O(3) position supports the defect model based on the mass action law with localized charge carriers and random oxygen vacancies located at the O(1) and O(3) sites, proposed to reproduce thermodynamic data of $Sr_3Fe_2O_{6+\delta}$.[15]

Besides, the localization of oxygen vacancies at the O(3) position is a strong enough evidence to understand the pathways for the oxygen ion migration mechanism, that should include jumps from the position O(3) to either a neighboring empty O(3′) site within the FeO_2 plane or a nearby empty O(1) site. Considering the available space, the $d_{O(1)-O(3)}$ and $d_{O(3)-O(3)'}$ jump distances and the increasing oxygen vacancy concentration with the series $Sr_3Fe_2O_{6+\delta}$ < $Sr_3FeCoO_{6+\delta}$ < $Sr_3FeNiO_{6+\delta}$, the ionic conductivity σ_{ion} should increase according to the relation $\sigma_{ion}^{Fe} < \sigma_{ion}^{Co} < \sigma_{ion}^{Ni}$.

The total expansions along the *a* and *c* directions of the $n = 2$ R-P phases $Sr_3FeMO_{6+\delta}$ (M = Fe, Co, Ni) have been determined. The results have been interpreted based on thermal effects associated to nonsymmetrical properties of the interatomic potential, and chemical effects associated to changes in the transition metal oxidation states and lattice distortions created by oxygen vacancies. The total expansion along the *c* direction was found to follow the series α_c(Fe) < α_c(Co) < α_c(Ni), which indicates that the chemical expansion prevails over the thermal expansion effect, while the combination of both effects is responsible for the maximum of the total expansion along the *a* axis for $Sr_3FeCoO_{6+\delta}$. The variations of bond distances with temperature show that the total expansion along the *c* axis, α_c, affects mainly the perovskite block while the width of the rock salt layers remains stable.

The average linear expansion coefficient, $\alpha_{ave} \approx {}^1/_3\ \alpha_{Vol}$, obtained for $Sr_3Fe_2O_{6+\delta}$, $Sr_3FeCoO_{6+\delta}$, and $Sr_3FeNiO_{6+\delta}$ were 19.9, 25.1, and 22.7 × 10^{-6} K^{-1}, respectively. These values are in the same range than those reported for the cobaltites.[40,41]

Acknowledgment. This work was supported by CNEA (Argentine Atomic Energy Commission), CONICET (Argentine Research Council) through PIP 5594, ANPCyT through PICT 03-12-14493 and PICT 06-00829 and Cooperation Program ECOS-SUD.

Supporting Information Available: The half-width (U,V,W) and asymmetry parameters, number of refined parameters in the

last cycle, and the number of reflections for $Sr_3FeMO_{6+\delta}$ (M = Fe, Co, Ni) are given in Table I. Tables II, III, and IV contain the oxygen occupancy of the O(1) and O(3) crystal sites, the total oxygen content, and refinement quality factors obtained from alternative models during the crystal structure refinement of $Sr_3FeMO_{6+\delta}$ (M = Fe, Co, Ni) (PDF). This material is available free of charge via the Internet at http://pubs.acs.org.